REPORT
by
The Ohio State University ElectroScience Laboratory
(Formerly Antenna Laboratory)
Columbus, Ohio 43212

Sponsor	National Aeronautics and Space Administration Office of Grants and Research Contracts Washington, D.C. 20546
Grant Number	NsG-448
Investigation of	Spacecraft Antenna Problems
Subject of Report	Radiation Pattern of a Ground-Plane Mounted Parallel-Plate Waveguide Analyzed by a Surface Integration Technique
Submitted by	Edward Pelton, David Wu and Roger Rudduck ElectroScience Laboratory Department of Electrical Engineering
Date	25 July 1968

ABSTRACT

The radiation pattern of a TEM mode parallel-plate waveguide mounted in an infinite ground plane is analyzed by a surface integration technique. The fields on the surface of integration are obtained by use of wedge diffraction theory and include plane wave diffraction plus first order interactions at the guide aperture. A derivation of the surface integral formulation is presented. The radiation patterns obtained by surface integration for the ground plane mounted guide compare favorably with other approximate methods and provide an improvement in accuracy as compared to the wedge diffraction method. Direct application of the theory to certain other related antenna geometries is possible.

TABLE OF CONTENTS

RADIATION PATTERN OF A GROUND-PLANE MOUNTED PARALLEL-PLATE WAVEGUIDE ANALYZED BY A SURFACE INTEGRATION TECHNIQUE

I. INTRODUCTION

Increased use of small aperture antennas for spacecraft and other airborne vehicle applications has created a need for developing improved techniques for their analysis. One of the important problems facing designers of such antennas lies in obtaining accurate radiation pattern information for a particular configuration. In general each configuration must be carefully analyzed, since the radiation pattern is strongly dependent on diffraction effects at the antenna aperture. Wedge diffraction theory has found extensive application in dealing with diffraction effects of various antenna configurations.[1,2,3] Although radiation pattern analysis based on direct application of wedge diffraction theory yields excellent results in many applications, it has been found that wedge diffraction does not yield accurate results in certain regions of the radiation pattern for narrow aperture antennas. Specifically, for aperture widths on the order of $\lambda/2$ or less, it was found by Yu and Rudduck[3] that wedge diffraction analysis does not accurately describe the pattern of a ground-plane mounted parallel-plate waveguide in the region near the plane of the aperture.

A surface integration technique presented by Wu[4] established a method of overcoming the limitation mentioned above. In Reference 4, which involved an analysis of a thin-walled parallel-plate waveguide, the validity of the surface integration technique was verified by comparing results with the known exact solution. The results were found to be in close agreement with the exact solution, and errors were due primarily to approximations used in obtaining the fields on the surface of integration.

In the present publication a surface integration technique will be employed in conjunction with wedge diffraction theory to improve the radiation pattern near the plane of the guide aperture for a ground-plane mounted guide. The formulation of an appropriate surface integral is presented in Section II. In Section III, the radiation pattern for a ground-plane mounted parallel-plate waveguide is obtained quite readily from the surface integral representation. There is no exact solution known for the ground-plane mounted guide considered here. The solution obtained in Section III is also approximate, due to approximations required in evaluation of the fields on the surface of integration. However, the results obtained by surface integration show good agreement with approximate results obtainable by the Fourier transform method. Thus the analyses employed in this publication provide a definite improvement in the accuracy of the pattern near the plane of the aperture, as compared to the results obtained previously by the application of the wedge diffraction method.

II. FORMULATION OF QUARTER-SPACE RADIATION IN TERMS OF A SURFACE INTEGRAL

In this section the radiation into the quarter-space $x > 0$ and $y > 0$ is expressed in terms of the fields on the planar surfaces S_1 and S_2 as shown in Fig. 1. Since only the two dimensional problem in which the fields are independent of z, is being considered, the radiation can be expressed in terms of the field on the positive x and y axes. Only the TM case is considered, i.e., the magnetic field is z-polarized.

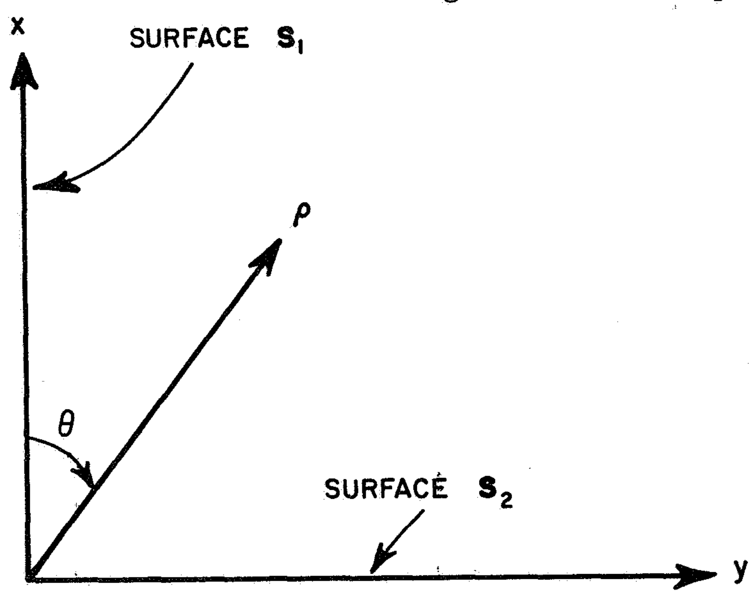

Fig. 1. Geometry of quarter-space radiation problem.

The magnetic field H satisfies the wave equation in the region $x > 0$, $y > 0$ and the wave equation is expressible as

$$(1) \qquad (\nabla^2 + k^2)H = 0$$

where $k = 2\pi/\lambda$ is the free-space propagation constant. The magnetic field H, may be expressed in general by use of Green's second identity for scalar fields giving

$$(2) \qquad H(\rho, \theta) = \int_0^{\infty} \left[H(x', 0) \frac{\partial G}{\partial y'} \bigg|_{y'=0} - G \frac{\partial H(x', y')}{\partial y'} \bigg|_{y'=0} \right] dx' - \int_0^{\infty} \left[H(0, y') \frac{\partial G}{\partial x'} \bigg|_{x'=0} - G \frac{\partial H(x', y')}{\partial x'} \bigg|_{x'=0} \right] dy'$$

where primed variables denote source coordinates.

The two-dimensional free space Green's function G_o is a valid Green's function for Eq. (2) where G_o is given by

$$(3) \qquad G_o = \frac{1}{4j} H_o^{(2)}(kr).$$

The quantity $H_o^{(2)}(kr)$ is the zero-th order Hankel function of the second kind. Equation (2) can be simplified if certain boundary conditions are imposed on the surfaces S_1 and S_2 shown in Fig. 1. The boundary conditions are chosen as

(a) $\qquad G = 0$ on S_1

(b) $\qquad \frac{\partial G}{\partial x'} = 0$ on S_2 .

Therefore Eq. (2) simplifies to

$$(4) \qquad H(\rho, \theta) = \int_0^{\infty} H(x'0) \frac{\partial G}{\partial y'} \bigg|_{y'=0} dx' + \int_0^{\infty} G \frac{\partial H(x' y')}{\partial x'} \bigg|_{x'=0} dy' .$$

In order to satisfy conditions (a) and (b), the required Green's function is given by

$$G = \frac{1}{4j}\left(H_o^{(2)}(kr_1) - H_o^{(2)}(k\,r_2) + H_o^{(2)}(k\,r_3) - H_o^{(2)}(k\,r_4)\right) \tag{5}$$

where r_1, r_2, r_3 and r_4 are the distances between the sources and the observation point as shown in Fig. 2. The Green's function of Eq. (5) can be derived by applying image theory to the 90° sector. It is noted that the Green's function of Eq. (5) corresponds to that for a 270° wedge with one surface a perfect magnetic conductor and the other a perfect electric conductor.

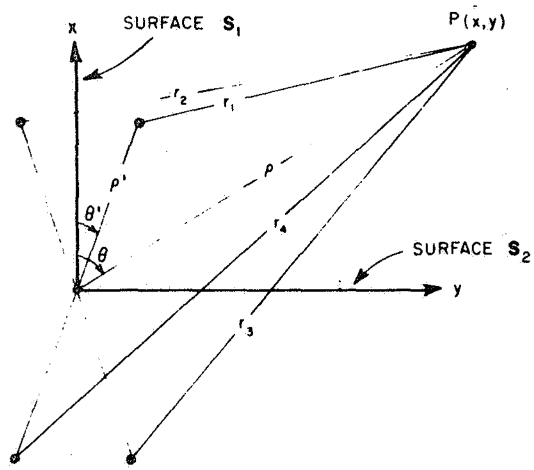

Fig. 2. Application of image theory.

The Green's function of Eq. (5) is put into a form valid for large values of ρ, since only the radiation pattern is of interest. For large values of ρ we have,

$$\begin{cases} r_1 \approx \rho - \rho' \cos(\theta-\theta') \\ r_2 \approx \rho - \rho' \cos(\theta+\theta') \\ r_3 \approx \rho + \rho' \cos(\theta+\theta') \\ r_4 \approx \rho + \rho' \cos(\theta-\theta') \end{cases} \tag{6}$$

Using the asymptotic form of the Hankel function, valid for large values of ρ, and approximating r_1, r_2, r_3, r_4 by ρ for magnitude and by Eq. (6) for phase, the Green's function is thus given by

$$(7) \qquad G \sim \frac{j\, e^{-j\left(k\rho+\frac{\pi}{4}\right)}}{2j\sqrt{2\pi k\rho}} \left[e^{+jk\rho'\cos(\theta-\theta')} - e^{+jk\rho'\cos(\theta+\theta')} + e^{-jk\rho'\cos(\theta+\theta')} - e^{-jk\rho'\cos(\theta-\theta')} \right]$$

$$= \frac{j\, e^{-j\left(k\rho+\frac{\pi}{4}\right)}}{\sqrt{2\pi k\rho}} \left[\sin(k\rho'\cos(\theta-\theta')) - \sin(k\rho'\cos(\theta+\theta')) \right] .$$

Therefore the Green's function evaluated on the y-axis is given by

$$(8) \qquad G\Big|_{x'=0} = G\Big|_{\theta'=\frac{\pi}{2}} \sim \frac{2j\, e^{-j\left(k\rho+\frac{\pi}{4}\right)}}{\sqrt{2\pi k\rho}} \sin(k\rho'\sin\theta) \quad .$$

And the normal derivation of the Green's function evaluated on the x-axis is given by

$$(9) \qquad \frac{\partial G}{\partial y'}\Big|_{y'=0} = \frac{1}{\rho}\frac{\partial G}{\partial \theta'}\Big|_{\theta'=0}$$

$$= \frac{2jk\, e^{-j\left(k\rho+\frac{\pi}{4}\right)}}{\sqrt{2\pi k\rho}} \sin\theta \cos(kx'\cos\theta) \quad .$$

Substituting Eqs. (8) and (9) into Eq. (4) and suppressing the factor

$$\frac{e^{-j\left(k\rho+\frac{\pi}{4}\right)}}{\sqrt{2\pi k\rho}} ,$$

the angular variation of the radiation pattern is given by

$$(10) \qquad R(\theta) = \int_0^\infty H(x'0)\ 2jk\ \sin\theta \cos(kx'\cos\theta)\ dx' + \int_0^\infty 2j \sin(ky'\sin\theta) \left.\frac{\partial H(x'y')}{\partial x'}\right|_{x'=0} dy' \quad .$$

For the application to be considered in the next section, the normal derivative of the magnetic field is zero on surface S_2. In this application with a perfect electric conductor coincident with surface S_2, Eq. (10) simplifies to

$$(11) \qquad R(\theta) = \int_0^\infty 2\ jk\ \sin\theta\, H(x', 0)\ \cos(kx'\cos\theta)\ dx' \quad .$$

This result is used in Section III to obtain the radiation pattern of the parallel-plate guide.

III. RADIATION PATTERN OF A PARALLEL-PLATE WAVEGUIDE MOUNTED IN AN INFINITE GROUND PLANE

The surface integration method presented in the last section is used here to obtain the TEM mode radiation pattern of a ground-plane mounted parallel-plate waveguide. The geometry to be considered is shown in Fig. 3, in which the surface of integration S extends along the x-axis. The TEM mode can be considered to be a section of a plane wave propagating parallel to the guide axis, with the electric field polarized perpendicular to the conducting walls. The observation point is assumed to be a large distance from the guide aperture (ρ large) and in the region $0 \leq \theta \leq 90°$. This region, due to the symmetry involved, describes the entire radiation pattern.

The exact solution for the radiation pattern of this geometry is not known. The technique presented here, although approximate, is thought to be quite accurate over the entire pattern, including the region near the ground plane for which the wedge diffraction method is inaccurate for narrow aperture widths.

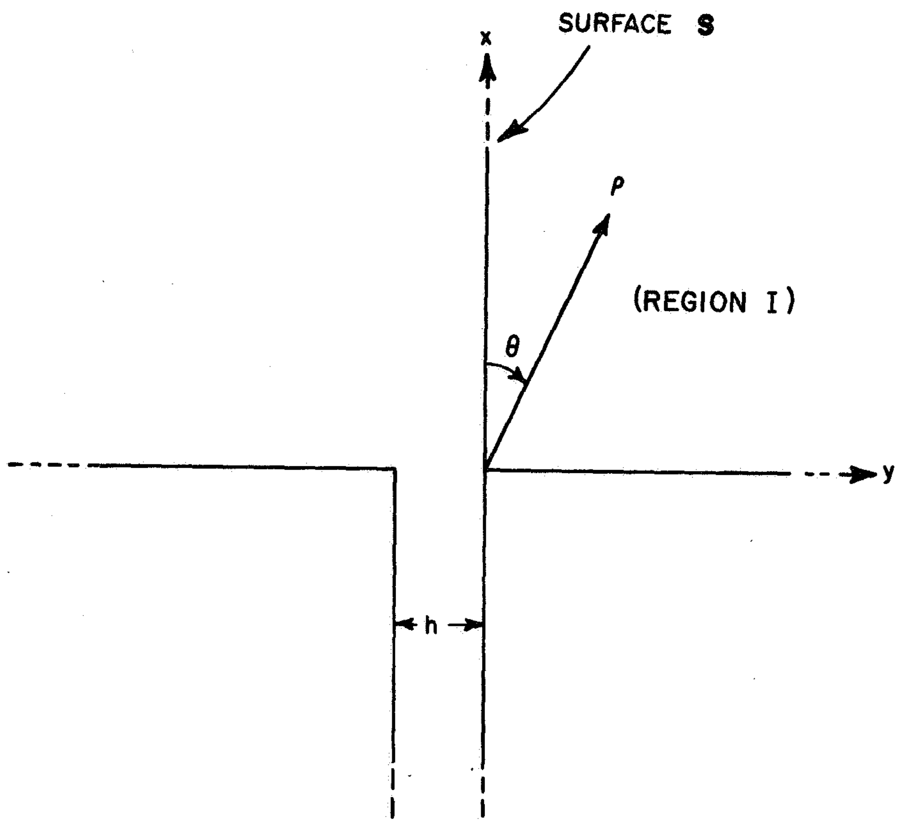

Fig. 3. Geometry of ground-plane mounted waveguide and the surface of integration.

A. Formulation Of The Fields On The Surface Of Integration

In order to carry out the surface integration indicated in Eq. (11), the total fields on the surface S, $H_T(x', 0)$, must be evaluated. By viewing the geometry of Fig. 3 as two right angle wedges, the fields on S can be formulated by use of the theory of wedge diffraction.[1] Thus wedge diffraction theory is employed in this analysis, with the total fields on S being approximated by the plane wave diffracted fields (singly diffracted fields), plus the diffracted fields due to first order interaction at the aperture (doubly diffracted fields). Although direct application of wedge diffraction theory does not always give accurate values for the doubly diffracted fields in all of Region I, it does give accurate values on the surface S, from which the surface integration approach can be employed to accurately evaluate the fields throughout Region I as shown in Fig. 3.

The singly diffracted fields on S, due to plane wave diffraction from edges 1 and 2 (denoted by A and B, respectively, in Fig. 4), can be expressed by use of the wedge diffraction function, $V_B(\rho, \phi, n)$, as

(12) $$H_1^{(1)}(x', 0) = V_B\left(r_1, \phi_1, \frac{3}{2}\right)$$

(13) $$H_2^{(1)}(x', 0) = V_B\left(x', \pi, \frac{3}{2}\right)$$

where $r_1 = \sqrt{h^2 + x'^2}$, $\phi_1 = \frac{\pi}{2} + \tan^{-1} \frac{x'}{h}$.

The subscripts 1, 2 denote edges 1 and 2, respectively, and the superscript 1 denotes singly diffracted fields.

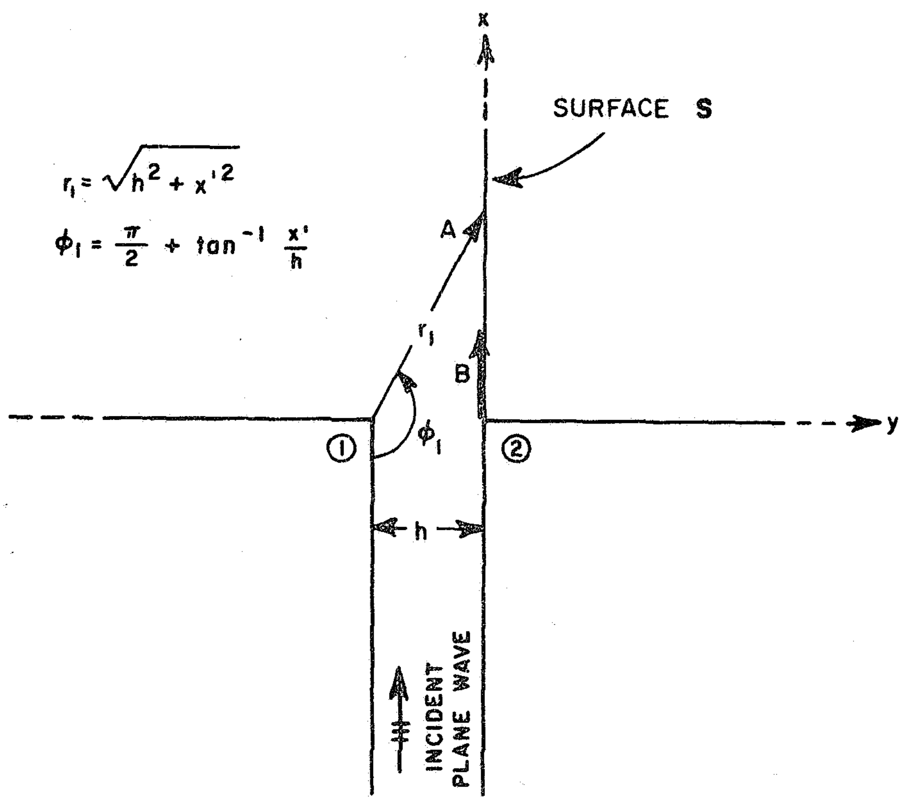

Fig. 4. Singly diffracted fields on the surface of integration, S.

In order to approximate the effect of the interaction between edges 1 and 2, the doubly diffracted fields on S must be considered. The doubly diffracted fields on S from one edge (1 or 2) are due to the singly diffracted wave incident from the opposite edge (2 or 1). Although the singly diffracted wave across the aperture deviates somewhat from a cylindrical wave for narrow guide widths, the uniform cylindrical wave approximation employed in the wedge diffraction method is quite good. According to wedge diffraction theory, a uniform line source placed at either edge 1 or 2 produces a cylindrical wave field in the direction of the opposite edge which is given by

$$V_B\left(r, \frac{\pi}{2}, \frac{3}{2}\right) \sim -\frac{1}{\sqrt{3}} \frac{e^{-j\frac{\pi}{4}}}{\sqrt{2\pi k}} \frac{e^{-jkr}}{\sqrt{r}} \quad . \tag{14}$$

The amplitude of this line source is

$$-\frac{1}{\sqrt{3}} \frac{e^{-j\frac{\pi}{4}}}{\sqrt{2\pi k}} \quad .$$

The doubly diffracted fields from edge 1 on the surface S (denoted by C in Fig. 5) are obtained in terms of cylindrical wave diffraction as

$$H_1^{(2)}(x', 0) = -\frac{1}{\sqrt{3}} \frac{e^{-j\frac{\pi}{4}}}{\sqrt{2\pi k}} \frac{e^{-jk(h+r_1)}}{\sqrt{h+r_1}} e^{jk\frac{hr_1}{h+r_1}} \times \left[V_B\left(\frac{hr_1}{h+r_1}, \alpha_1, \frac{3}{2}\right) + V_B\left(\frac{hr_1}{h+r_1}, \pi+\alpha_1, \frac{3}{2}\right)\right] \tag{15}$$

where $r_1 = \sqrt{h^2 + x'^2}$ and $\alpha_1 = \tan^{-1} \frac{x'}{h}$.

Similarly, the doubly diffracted fields from edge 2 on S (denoted by D in Fig. 5) are given by

$$H_2^{(2)}(x', 0) = \frac{-e^{-j\frac{\pi}{4}}}{\sqrt{3}\sqrt{2\pi k}} \frac{e^{-jk(h+x')}}{\sqrt{h+x'}} e^{jk\frac{hx'}{h+x'}} \times \left[V_B\left(\frac{hx'}{h+x'}, \frac{\pi}{2}, \frac{3}{2}\right) + V_B\left(\frac{hx'}{h+x'}, \frac{3\pi}{2}, \frac{3}{2}\right)\right] \quad . \tag{16}$$

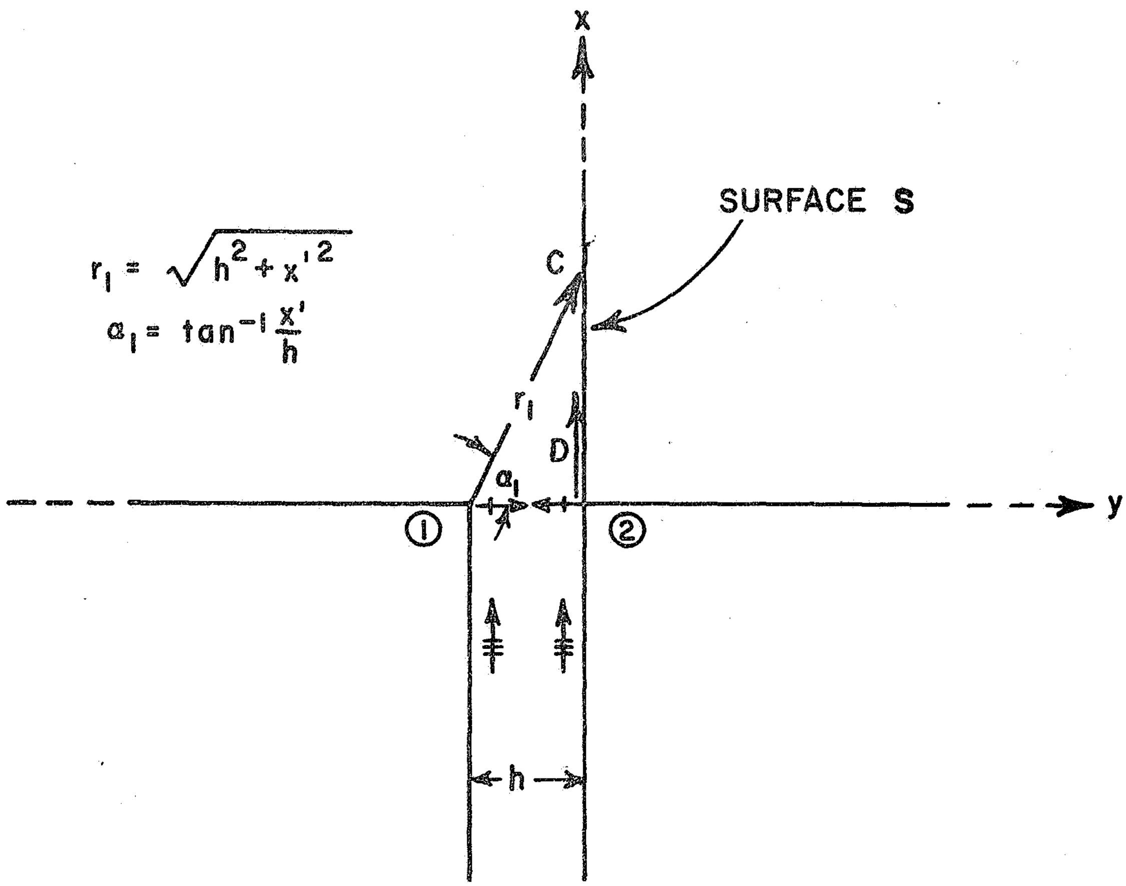

Fig. 5. Doubly diffracted fields on the surface of integration, S.

The sum of Eqs. (12), (13), (15) and (16) give the total fields on S to the order of approximation considered here. However, since the integration on S extends to infinity, it is necessary to develop far-field (x' large) representations for these fields which permit analytic evaluation of the integral beyond some distance $x' = x_m$. It can be shown that for values of $x' \geq x_m$, where x_m is on the order of 20λ, the singly diffracted fields from both edges 1 and 2 on the surface S can be expressed by

$$(17) \qquad H_1^{(1)}(x', 0) + H_2^{(1)}(x', 0) = \frac{e^{-j\frac{\pi}{4}}}{\sqrt{2\pi k}} \left(\frac{2}{3\sqrt{3}} + jkh\right) \frac{e^{-jk\sqrt{x'^2 + \left(\frac{h}{2}\right)^2}}}{\left[x'^2 + \left(\frac{h}{2}\right)^2\right]^{\frac{1}{4}}} .$$

This relation can be further simplified, for $x_m >> h$, by approximating the magnitude decay by

$$\frac{1}{\left[(x')^2 + \left(\frac{h}{2}\right)^2\right]^{\frac{1}{4}}} \approx \frac{1}{\sqrt{x'}}$$

and the phase variation by

$$e^{-jk\sqrt{x'^2 + \left(\frac{h}{2}\right)^2}} \approx e^{-jkx'} \left[1 - j\left(\frac{h}{2}\right)^2 \frac{k}{2x'}\right] .$$

Employing these approximations, the singly diffracted fields on S, for $x' \geq x_m$, are given by

(18) $$H_1^{(1)}(x', 0) + H_2^{(1)}(x', 0) = K_1 \left(1 - j\frac{kh^2}{8x'}\right)\frac{e^{-jkx'}}{\sqrt{x'}}$$

where K_1 is a constant defined as

(19) $$K_1 = \frac{e^{-j\frac{\pi}{4}}}{\sqrt{2\pi k}} \left(\frac{2}{3\sqrt{3}} + jkh\right) .$$

Approximations for the doubly diffracted fields from edges 1 and 2 on S, valid for $x' \geq x_m$, can be obtained from Eqs. (15) and (16) as

(20) $$H_1^{(2)}(x', 0) = K_2 \left(1 - \frac{jkh^2}{2x'}\right) \frac{e^{-jkx'}}{\sqrt{x'}}$$

(21) $$H_2^{(2)}(x', 0) = K_2 \frac{e^{-jkx'}}{\sqrt{x'}}$$

with K_2 being a constant defined by

(22) $$K_2 = -\frac{e^{-j\frac{\pi}{4}}}{\sqrt{3}\sqrt{2\pi k}} \left[V_B\left(h, \frac{\pi}{2}, \frac{3}{2}\right) + V_B\left(h, \frac{3\pi}{2}, \frac{3}{2}\right)\right] .$$

B. Obtaining The Radiation Pattern By Surface Integration

The radiation pattern can be obtained by substituting the appropriate expressions for the fields on the surface S, developed in the last section, into Eq. (11). Since, as indicated previously, the integration is to be split into the two intervals $(0 \le x' \le x_m)$ and $(x_m \le x' \le \infty)$, Eq. (11) is rewritten here as

$$(23) \qquad R_T(\theta) = \int_0^{x_m} jk \sin\theta \, H_T(x', 0) \left[2 \cos(kx' \cos\theta)\right] dx'$$

$$+ \int_{x_m}^{\infty} jk \sin\theta \, H_T(x', 0) \, e^{jkx' \cos\theta} \, dx'$$

$$+ \int_{x_m}^{\infty} jk \sin\theta \, H_T(x', 0) \, e^{-jkx' \cos\theta} \, dx'$$

where the last two terms are obtained by replacing the cosine factor by its exponential representation. Further, it is convenient to separate Eq. (23) into four components denoted by

$$(24) \qquad R_T(\theta) = R_1^{(1)}(\theta) + R_2^{(1)}(\theta) + R_1^{(2)}(\theta) + R_2^{(2)}(\theta)$$

where each component of Eq. (24) is due to the corresponding field terms $H_1^{(1)}$, $H_2^{(1)}$, $H_1^{(2)}$, $H_2^{(2)}$ on S.

The integration in the first term of Eq. (23) is evaluated numerically on a computer, while use of the far-zone relations Eqs. (18), (20), and (21) in the second and third terms involves integrations of the form

$$\int_{x_m}^{\infty} \frac{e^{-jk(1 \pm \cos\theta)\, x'}}{\sqrt{x'}} \, dx' \quad ; \quad \int_{x_m}^{\infty} \frac{e^{-jk(1 \pm \cos\theta) x'}}{(x')^{3/2}} \, dx'$$

which can be evaluated by use of the Fresnel integral. The form of the Fresnel integral used here is

$$(25) \qquad F(x) = \frac{1}{\sqrt{2\pi}} \int_x^{\infty} \frac{e^{-jt}}{\sqrt{t}}\, dt$$

where $F(0) = 1/\sqrt{2}\ e^{-j\,\pi/4}$. The required integrations are then defined in terms of the Fresnel integral as

$$(26) \qquad F_1(x_m, \theta) = \int_{x_m}^{\infty} \frac{e^{-jk[1+\cos\theta]\,x'}}{\sqrt{x'}}\, dx'$$

$$= \sqrt{\frac{2\pi}{k(1+\cos\theta)}}\ F\,[k\,x_m(1+\cos\theta)]$$

$$(27) \qquad F_2(x_m, \theta) = \int_{x_m}^{\infty} \frac{e^{-jk[\,1+\cos\theta]\,x'}}{(x')^{3/2}}\, dx'$$

$$= 2\left\{\frac{e^{-jk(1+\cos\theta)x_m}}{\sqrt{x_m}} - j\sqrt{2\pi\,k(1+\cos\theta)}\right.$$

$$\left. \times\ F\,[k\,x_m(1+\cos\theta)]\right\}.$$

The components of the radiation pattern as defined by Eq. (24) can now be expressed explicitly in terms of the numerical integration of the fields on S over the interval $0 \rightarrow x_m$, and the integral definitions of Eqs. (26) and (27). The portion of the radiation pattern due to singly diffracted fields from edges 1 and 2 can be written as

$$(28) \qquad R_1^{(1)}(\theta) + R_2^{(1)}(\theta) = \int_0^{x_m} jk\,\sin\theta\,[H_1^{(1)}(x', 0) + H_2^{(1)}(x', 0)]$$

$$\times\ [\,2\,\cos(kx'\cos\theta)\,]\ dx'$$

$$+\ jk\,\sin\theta\,K_1[\,F_1(x_m, \pi+\theta) - j\,\frac{kh^2}{8}\ F_2(x_m, \pi+\theta)]$$

$$+\ jk\,\sin\theta\,K_1[\,F_1(x_m, \theta) - j\frac{kh^2}{8}\ F_2(x_m, \theta)\,]$$

where Eqs. (12) and (13) are the appropriate expressions for use in the integrand of the first term. In a similar manner, the contributions to the radiation pattern of the doubly diffracted fields from edges 1 and 2, respectively, are given by

$$
R_1^{(2)}(\theta) = \int_0^{x_m} jk \sin\theta \, H_1^{(2)}(x', 0) \, [2 \cos(kx' \cos\theta)] \, dx' \tag{29}
$$

$$
+ jk \sin\theta \, K_2 \left[F_1(x_m, \pi+\theta) - j\frac{kh^2}{2} F_2(x_m, \pi+\theta) \right]
$$

$$
+ jk \sin\theta \, K_2 \left[F_1(x_m, \theta) - j\frac{kh^2}{2} F_2(x_m, \theta) \right]
$$

$$
R_2^{(2)}(\theta) = \int_0^{x_m} jk \sin\theta \, H_2^{(2)}(x', 0) \, [2 \cos(kx' \cos\theta)] \, dx' \tag{30}
$$

$$
+ jk \sin\theta \, K_2 \left[F_1(x_m, \pi+\theta) + F_1(x_m, \theta) \right] \quad .
$$

The appropriate expressions for the fields on S in the first terms of Eqs. (29) and (30) are those of Eqs. (15) and (16), respectively. The total radiation pattern, as indicated by Eq. (24), is obtained by taking the sum of Eqs. (28), (29) and (30).

The quantity x_m, in these equations, is a fixed distance in wavelengths for a given waveguide width. The minimum suitable value for x_m varies with waveguide width, however, and if the value of x_m is not chosen large enough , inaccurate results are obtained. As mentioned previously, a value of 20 wavelengths is usually sufficient for guide widths $h \leq 1\lambda$.

C. Results

Radiation patterns have been obtained numerically by programming the surface integral formulation of the last section on a digital computer. A statement listing of the computer program used is presented in Appendix A. This program makes extensive use of a newly developed subroutine for evaluation of the wedge diffraction function, $V_B(\rho, \phi, n)$. Appendix B contains a brief account of the theory used in the subroutine and a computer statement listing.

Radiation pattern calculations for the ground-plane mounted waveguide are shown graphically in Figs. 6 through 11, for six selected waveguide widths in the 0.2 to 0.8 wavelength range. These figures show four sets of calculations for each of the chosen guide widths. Two of these were obtained by the surface integration method, a third set of data is due to calculations made using the Fourier transform formulation of Nussenzveig[5] and the fourth set was obtained by the wedge diffraction method. The latter two sets of data are included to show a comparison between the results of the surface integration method and results obtained by other methods. All of the results are normalized to the on-axis value, $R(\theta = 0°)$, of Eq. (24). The two surface integration calculations differ only in that one of them was obtained by omitting the doubly diffracted term from edge 1 (i.e., $R_I^{(2)}$) in Eq. (24). The two different results indicate the effect of the number of diffraction components in the calculation.

Figure 8 shows a case of very close agreement in results. Table I, opposite the figure, presents both magnitude and phase calculations as an aid in comparing these results. The phase values in the table are referenced to the center of the waveguide aperture.

IV. CONCLUSIONS

The radiation patterns obtained by applying the surface integration technique to the ground-plane mounted parallel-plate waveguide geometry compare favorably with approximate results obtained by use of the Fourier transform method which includes the dominant mode and the next two higher order modes. Surface integration, as employed here provides an improvement in pattern accuracy over the wedge diffraction analysis. Specifically the technique improves pattern accuracy in the region near the plane of the aperture for waveguide widths on the order of $\lambda/2$ or less. In the region near the guide axis, the surface integration technique and the wedge diffraction method yield essentially the same results. The numerical calculations involved in the surface integration technique appear quite lengthy. However, using the programs presented in Appendices A and B, each pattern calculation shown in Figs. 6 through 11 required only about 1.5 minutes of IBM 7094 time.

Although the details of the analysis contained in this publication are limited to consideration of a parallel-plate waveguide mounted in an infinite ground plane, the technique can be applied to other configurations. For example, other parallel-plate waveguide geometries such as those with arbitrary truncation angles and arbitrary wedge angles can be treated. It also appears that the surface integration technique can be extended to treat more general configurations such as waveguides and slots mounted on finite ground planes or on curved surfaces.

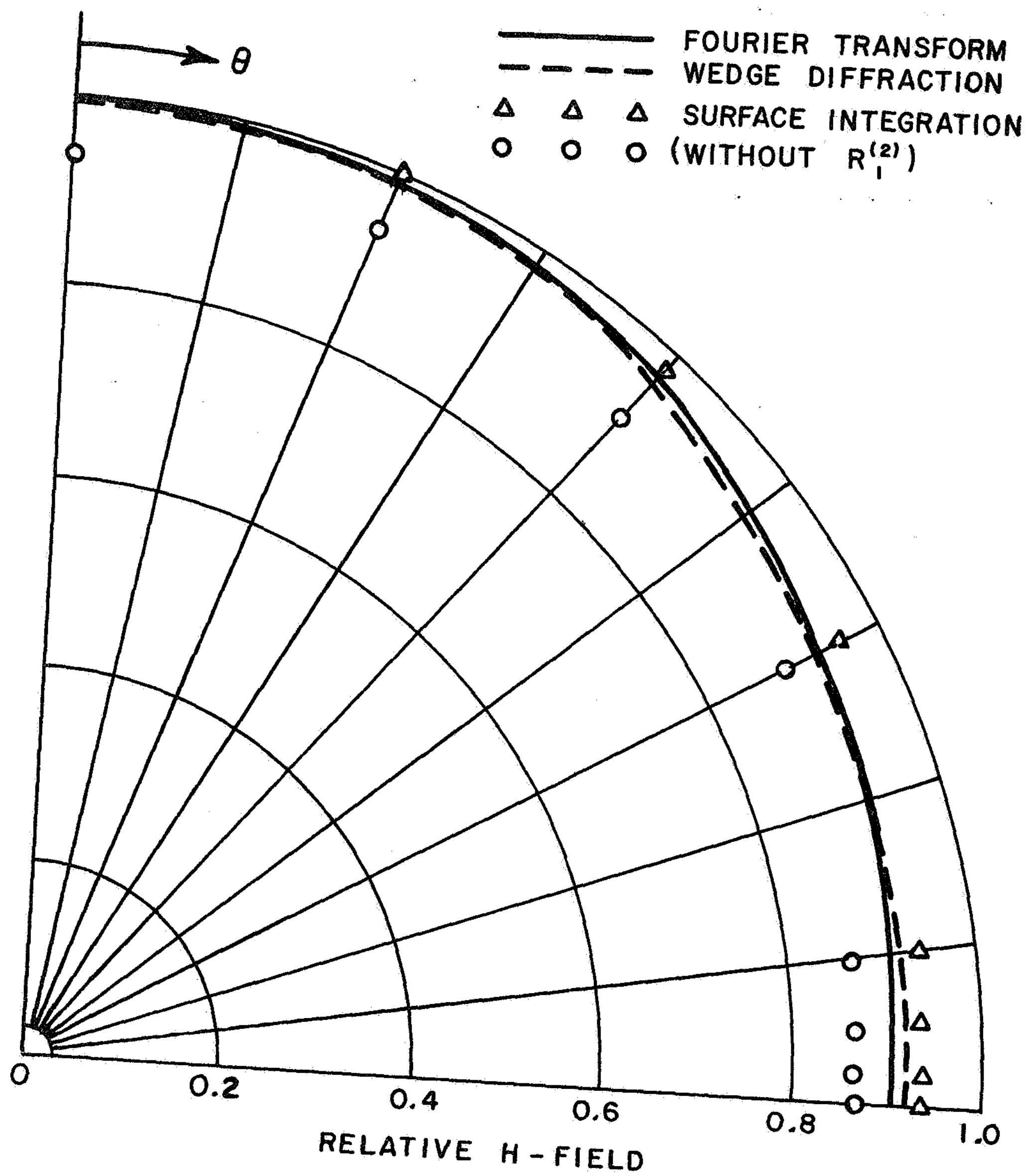

Fig. 6 Radiation pattern for TEM mode parallel-plate waveguide mounted in an infinite ground plane ($h/\lambda = 0.2228$).

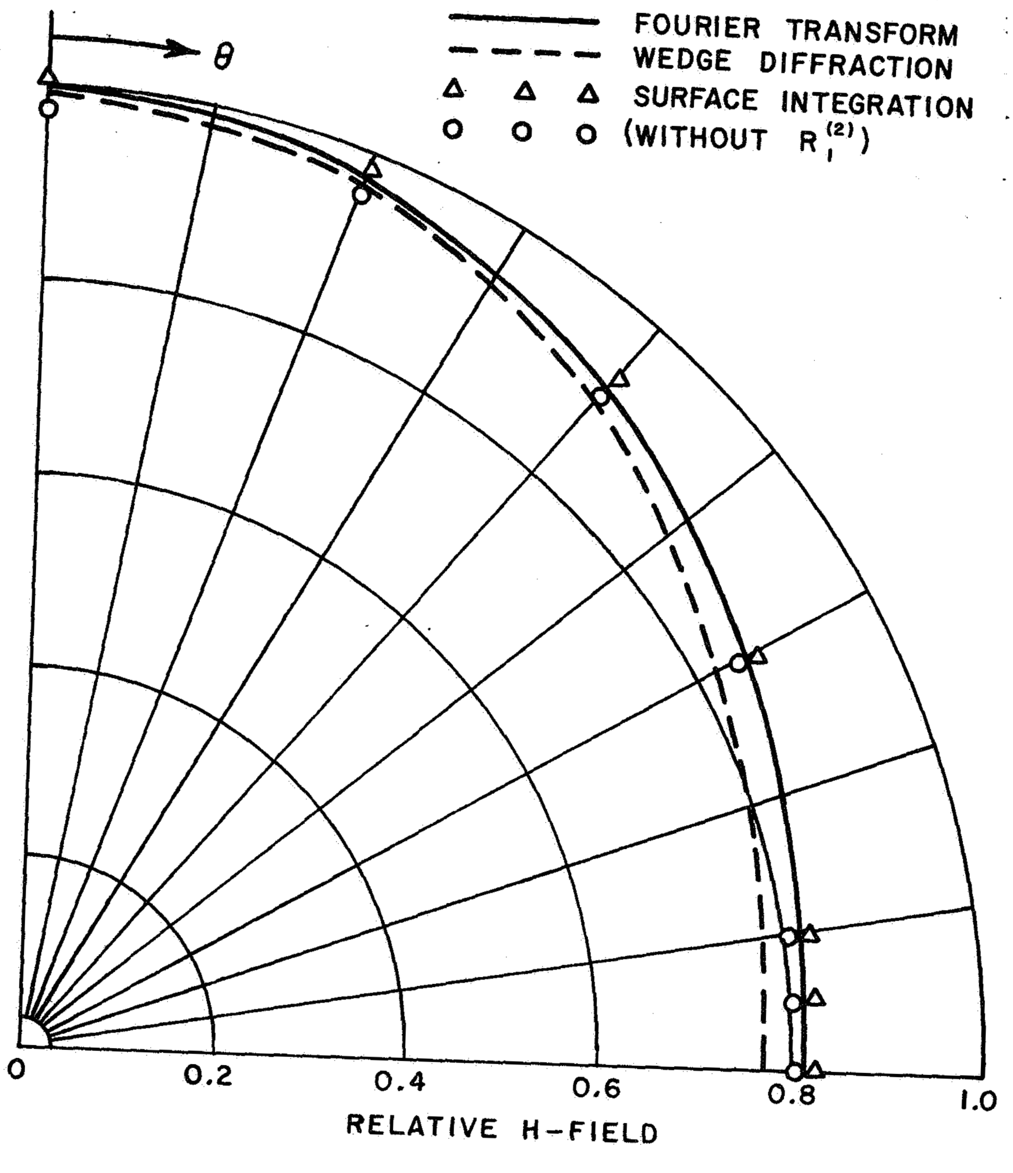

Fig. 7. Radiation pattern for TEM mode parellel-plate waveguide mounted in an infinite ground plane ($h/\lambda = 0.3183$).

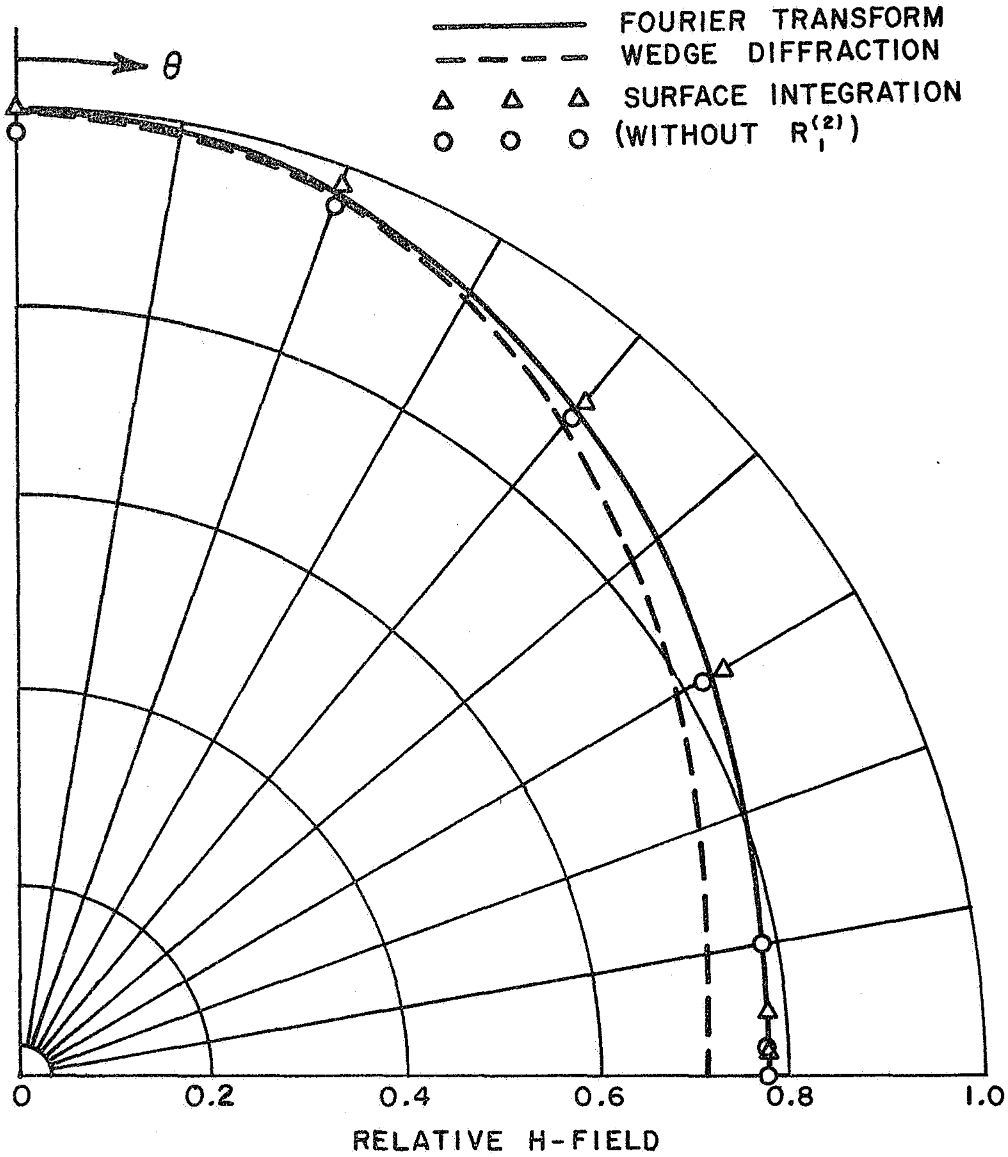

Fig. 8. Radiation pattern for TEM mode parallel-plate waveguide mounted in an infinite ground plane (h/λ = 0.3501).

TABLE I

($h/\lambda = 0.3501$)

	Fourier Transform Method		Surface Integration		Surface Integration Without $R_1^{(2)}$ term		Wedge Diffraction	
Theta in Degrees	Magnitude	Phase in Degrees	Magnitude	Phase in Degrees	Magnitude	Phase in Degrees	Magnitude	Phase in Degrees
0	1.000	76.7	1.000	76.5			1.0	76.5
20	0.972	76.8	0.974	76.4	0.960	79.0	0.967	76.6
40	0.904	77.2	0.908	76.4	0.899	79.5	0.884	76.7
60	0.829	77.6	0.833	76.5	0.829	80.2	0.789	76.0
80	0.782	77.9	0.785	76.7	0.783	80.6	0.725	73.4
85			0.780	76.7	0.779	80.7		
88			0.778	76.7				
90	0.776	78.0	0.778	76.7	0.777	80.7	0.700	80.3

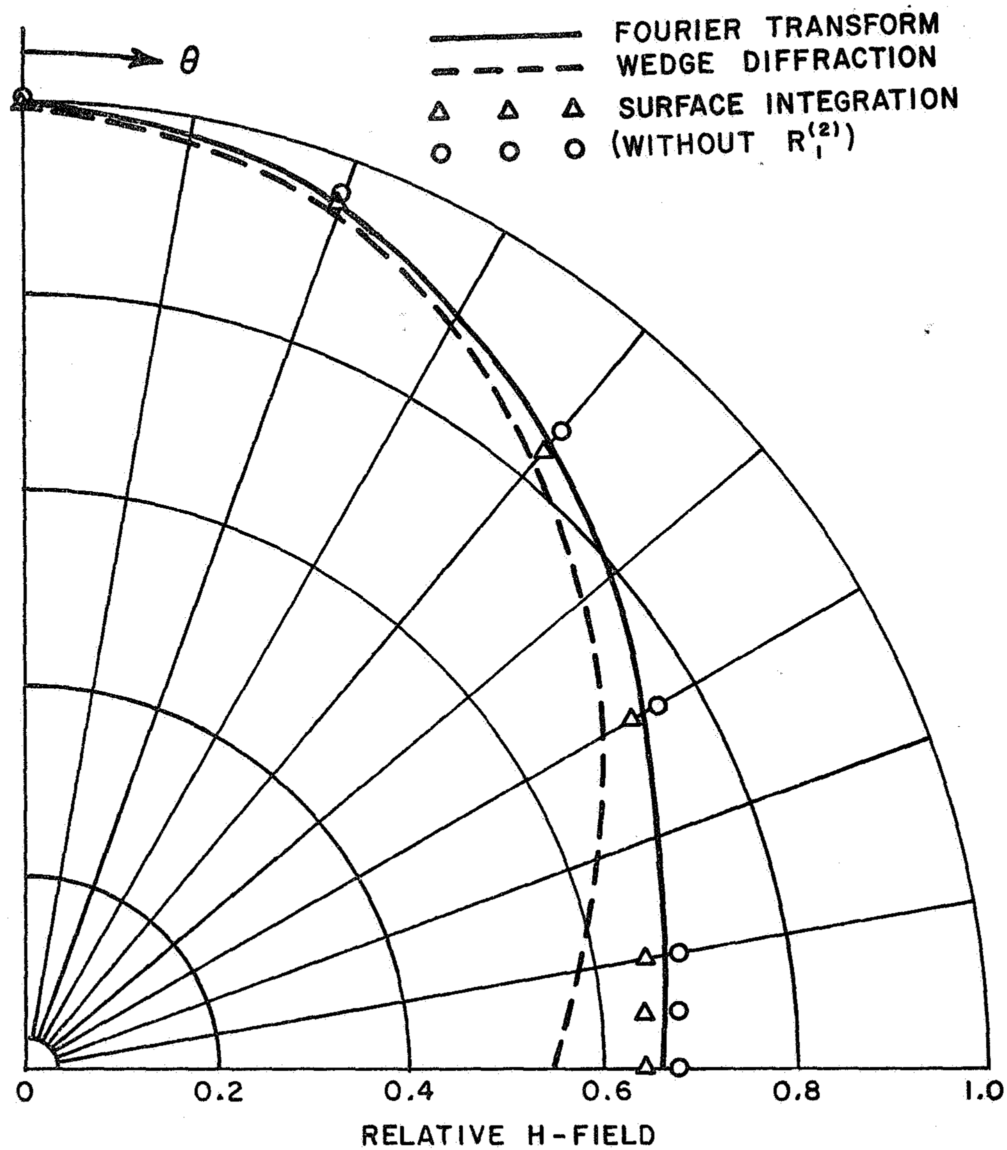

Fig. 9. Radiation pattern for TEM mode parallel-plate waveguide mounted in an infinite ground plane ($h/\lambda = 0.4456$)

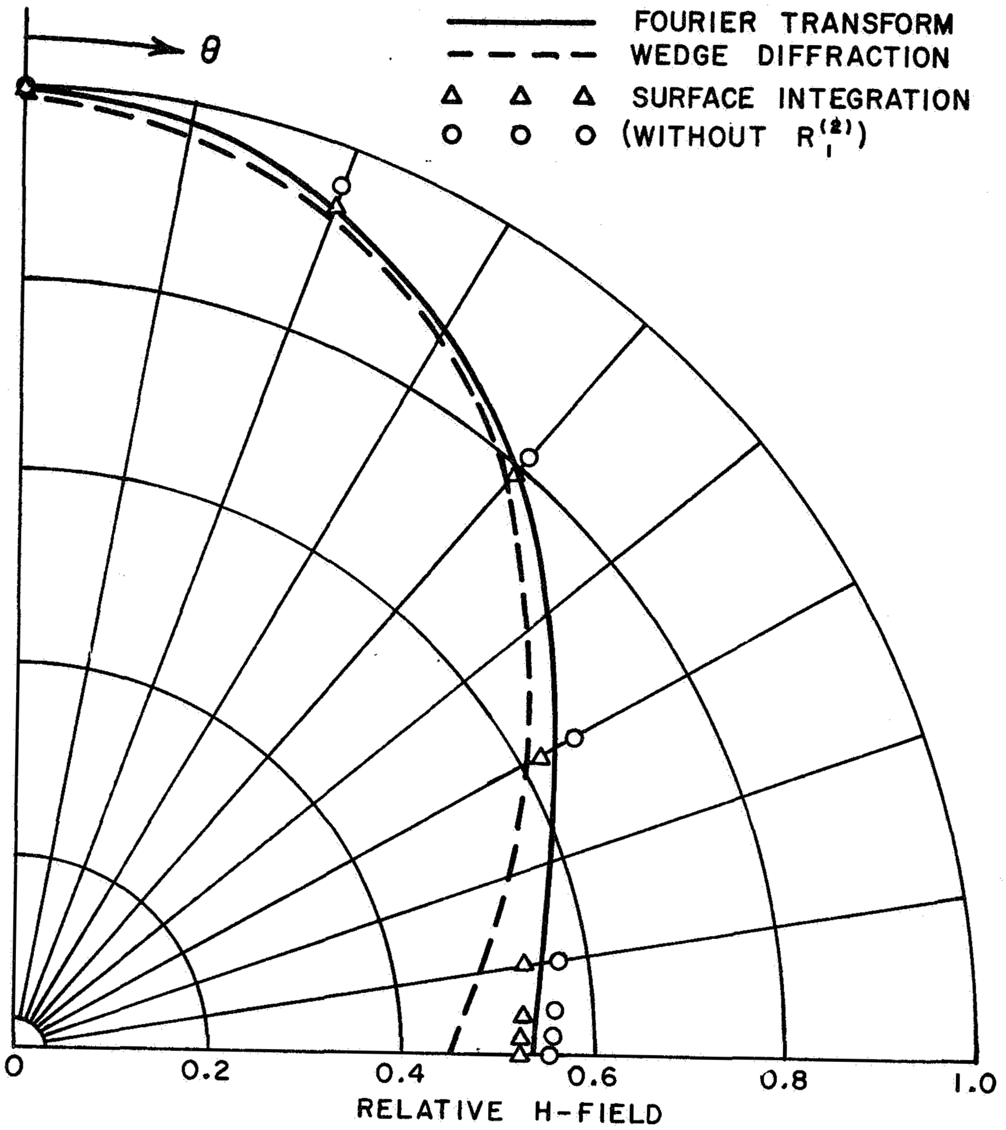

Fig 10. Radiation pattern for TEM mode parallel-plate waveguide mounted in an infinite ground plane (h/λ = 0.5411).

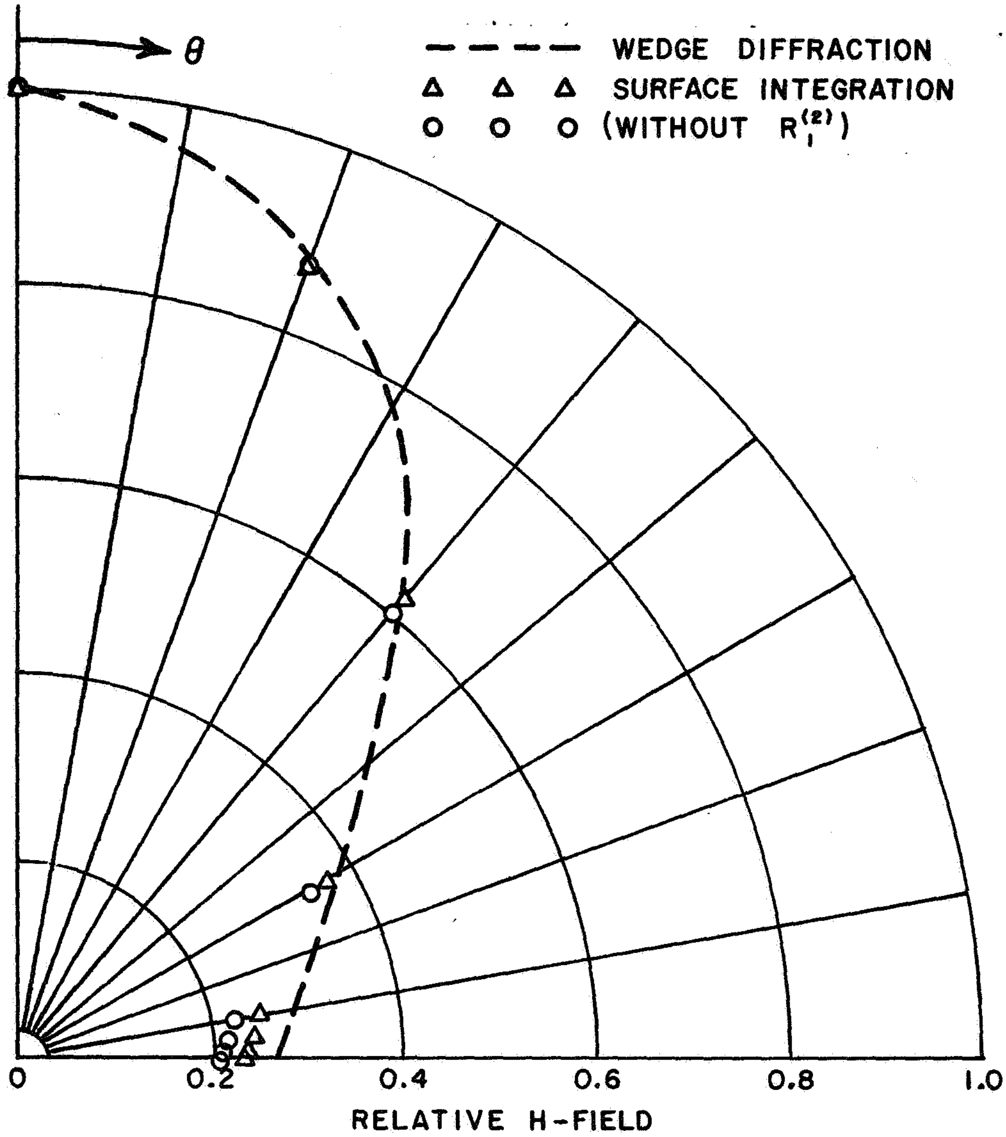

Fig. 11 Radiation pattern for TEM mode parallel-plate waveguide mounted in an infinite ground plane ($h/\lambda = 0.8$).

APPENDIX A

The Fortran IV program used for the numerical calculation of the radiation pattern for the ground-plane mounted parallel-plate waveguide is presented in this Appendix. The program was run on an IBM 7094 computer using the Purdue University Fast Fortran Translator (PUFFT) compiler.

It has been found that, for the point-by-point integration over the interval $0 \rightarrow x_m$, an x_m value of 10 wavelengths is sufficient for waveguide widths up to 0.5 wavelengths. An x_m value of 20 wavelengths gives good results for guide widths between 0.5 and 0.8 wavelengths. These values were employed in the computer calculations.

```
$EXECUTE        PUFFT
$PUFFT    400
      COMPLEX VBT,D90,CK2,CK1,FI2,FI3,F1I2A,F2I2A,CI2A,DELI21,PCN,DELI2,
     2R2,CI3A,PCP,DELI3,R3
      COMPLEX R90W,R90WO
      DIMENSION R1R(20),BER(20),R1U(20),BEU(20),R2R(20),R2U(20),R3R(20),
     2R3U(20),RRE(20),RU(20)
      FN=1.5
      PI=3.1415927
      TPI=2.0*PI
      READ(5,9) NUMCAS
 9    FORMAT (I2)
 11   NUMCAS=NUMCAS-1
      READ(5,17) H,AINC,NF
 17   FORMAT(2F10.7,I5)
      A=0.0
      B=1.0
      CALL ZINTG (R1R,R1U,A,B,H,AINC,NF)
 21   A=B
      B=A+1.0
      CALL ZINTG (BER,BEU,A,B,H,AINC,NF)
      DO 41 N=1,NF
      R1R(N)=R1R(N)+BER(N)
      R1U(N)=R1U(N)+BEU(N)
      WRITE(6,3) N,R1R(N),R1U(N)
 3    FORMAT(1H ,2HN=,I5,5X,7HR1R(N)=,E15.8,5X,7HR1U(N)=,E15.8)
      WRITE(6,13) BER(N),BEU(N)
 13   FORMAT(1H ,7HBER(N)=,E15.8,5X,7HBEU(N)=,E15.8)
 41   CONTINUE
      IF(A.LT.3.9) GO TO 21
      XM=B
      WRITE(6,5) XM
 5    FORMAT(1H ,3HXM=,F10.7)
      PH90=90.0
      PH270=270.0
      CALL VB (R90,U90,H,PH90,FN)
      CALL VB (R270,U270,H,PH270,FN)
      VBT=CMPLX(R90+R270,U90+U270)
      D90=((1.0/FN*SIN(PI/FN))/(COS(PI/FN)-COS(PI/(2.0*FN))))*(CEXP(CMPL
     2X(0.0,-PI/4.0))/TPI)
      CK2=D90*VBT
      CK1=CMPLX(1.0/(FN*SQRT(3.0)),TPI*H)*CEXP(CMPLX(0.0,-PI/4.0))/TPI
      DO 42 N=1,NF
      THETA=(FLOAT(N)-1.0)*AINC*PI/180.0
      IF(N.LT.4) THETA=THETA/2.0
      IF(N.EQ.5) THETA=FLOAT(N)*AINC*PI/180.0
      IF(N.EQ.6) THETA=FLOAT(N+1)*AINC*PI/180.0
      IF(N.EQ.7) THETA=2.0*PI/180.0
      CST=COS(THETA)
      STN=TPI*(1.0-SIN(THETA))
      F1I2A=TPI*CMPLX(0.0,CST)
      F2I2A=CK1+2.0*CK2
      X2=SQRT(STN*XM)
      CALL FRNELS (C,S,X2)
      C2=(0.5-C)/SQRT(STN/TPI)
      S2=(S-0.5)/SQRT(STN/TPI)
      FI2=CMPLX(C2,S2)
      CI2A=F1I2A*F2I2A*FI2
      DELI21=((PI*H)**2)*(CK1+4.0*CK2)*CST
      PCN=CEXP(CMPLX(0.0,-(STN*XM)))/SQRT(XM)
      DELI2=DELI21*(PCN-CMPLX(0.0,STN)*FI2)
      WRITE(6,23) N,DELI2
 23   FORMAT(1H ,2HN=,I5,5X,6HDELI2=,2E15.8)
      R2=CI2A+DELI2
```

```
      R2R(N)=REAL(R2)
      R2U(N)=AIMAG(R2)
      WRITE(6,8) N,R2R(N),R2U(N)
8     FORMAT(1H ,2HN=,I5,5X,7HR2R(N)=,E15.8,5X,7HR2U(N)=,E15.8)
      STP=TPI*(1.0+SIN(THETA))
      X3=SQRT(STP*XM)
      CALL FRNELS (C,S,X3)
      C3=(0.5-C)/SQRT(STP/TPI)
      S3=(S-0.5)/SQRT(STP/TPI)
      FI3=CMPLX(C3,S3)
      CI3A=F1I2A*F2I2A*FI3
      PCP=CEXP(CMPLX(0.0,-(STP*XM)))/SQRT(XM)
      DELI3=DELI21*(PCP-CMPLX(0.0,STP)*FI3)
      WRITE(6,24) N,DELI3
24    FORMAT(1H ,2HN=,I5,5X,6HDELI3=,2E15.8)
      R3=CI3A+DELI3
      R3R(N)=REAL(R3)
      R3U(N)=AIMAG(R3)
      WRITE(6,10) R3R(N),R3U(N)
10    FORMAT(1H ,19X,7HR3R(N)=,E15.8,5X,7HR3U(N)=,E15.8)
      R23R=R2R(N)+R3R(N)
      R23U=R2U(N)+R3U(N)
      WRITE(6,12) R23R,R23U
12    FORMAT(1H ,27X,5HR23R=,E15.8,5X,5HR23U=,E15.8)
      RRE(N)=R1R(N)+R2R(N)+R3R(N)
      RU(N)=R1U(N)+R2U(N)+R3U(N)
42    CONTINUE
      DO 43 N=1,NF
      RTHETM=SQRT(RRE(N)**2+RU(N)**2)
      RTHETP=ATAN2(RU(N),RRE(N))*180.0/PI
      R90W=-SQRT(2.0)*PI*(CK1+2.0*CK2)*CMPLX(1.0,1.0)
      R90WO=-SQRT(2.0)*PI*(CK1+CK2)*CMPLX(1.0,1.0)
      R90WM=SQRT(REAL(R90W)**2+AIMAG(R90W)**2)
      R90WOM=SQRT(REAL(R90WO)**2+AIMAG(R90WO)**2)
      R90WP=ATAN2(AIMAG(R90W),REAL(R90W))*180.0/PI
      R90WOP=ATAN2(AIMAG(R90WO),REAL(R90WO))*180.0/PI
      RTHTMN=RTHETM/R90WM
      RTHTPN=RTHETP/R90WP
      THETA=(FLOAT(N)-1.0)*AINC
      IF(N.LT.4) THETA=THETA/2.0
      IF(N.EQ.5) THETA=FLOAT(N)*AINC
      IF(N.EQ.6) THETA=FLOAT(N+1)*AINC
      IF(N.EQ.7) THETA=2.0
      WRITE(6,4) THETA,RRE(N),RU(N)
4     FORMAT (1H ,6HTHETA=,F10.5,5X,7HRRE(N)=,E15.8,5X,6HRU(N)=,E15.8)
      WRITE(6,7) RTHETM,RTHETP
7     FORMAT(1H ,23X,7HRTHETM=,E15.8,5X,7HRTHETP=,E15.8)
      WRITE(6,16) RTHTMN,RTHTPN
16    FORMAT(1H ,23X,7HRTHTMN=,E15.8,5X,7HRTHTPN=,E15.8)
      WRITE(6,18) R90WM,R90WP
18    FORMAT(1H ,23X,6HR90WM=,E15.8,5X,6HR90WP=,E15.8)
      WRITE(6,19) R90WOM,R90WOP
19    FORMAT(1H ,23X,7HR90WOM=,E15.8,5X,7HR90WOP=,E15.8)
      WRITE(6,20) R90W,R90WO
20    FORMAT(1H ,23X,5HR90W=,2E15.8,5X,6HR90WO=,2E15.8)
43    CONTINUE
      IF(H.LT.0.5.AND.XM.LT.9.9) GO TO 21
      IF(H.GE.0.5.AND.XM.LT.19.9) GO TO 21
      IF(NUMCAS.GT.0) GO TO 11
      STOP
      END
      SUBROUTINE ZINTG (ZINTGR,ZINTGU,A,B,H,AINC,NF)
      DIMENSION ZJR(20),ZJU(20),ZLR(20),ZLU(20),SR(20),SU(20),ZJOR(20),Z
     2JOU(20),ERRRE(20),ERRU(20),ZINTGR(20),ZINTGU(20),FFAR(20),FFBR(20)
```

```
     3,FFAU(20),FFBU(20),FFQR(20),FFQU(20)
      CALL FNCTN (FFAR,FFAU,H,AINC,NF,A)
      CALL FNCTN (FFBR,FFBU,H,AINC,NF,B)
      DO 114 N=1,NF
      ZJR(N)=B-A
      ZJU(N)=0.0
      ZH=0.5*(B-A)
      ZLR(N)=ZH*(FFAR(N)+FFBR(N))
  114 ZLU(N)=ZH*(FFAU(N)+FFBU(N))
      NN=1
      NLF=5
      IF(B.LE.1.0) NLF=6
      DO 136 L=1,NLF
      DO 118 N=1,NF
      SR(N)=0.0
  118 SU(N)=0.0
      DO 124 M=1,NN
      FI=FLOAT(M)
      Q=(2.0*FI-1.0)*ZH+A
      CALL FNCTN (FFQR,FFQU,H,AINC,NF,Q)
      DO 124 N=1,NF
      SR(N)=SR(N)+FFQR(N)
      SU(N)=SU(N)+FFQU(N)
  124 CONTINUE
      DO 132 N=1,NF
      ZJOR(N)=ZJR(N)
      ZJOU(N)=ZJU(N)
      ZJR(N)=ZLR(N)+4.0*ZH*SR(N)
      ZJU(N)=ZLU(N)+4.0*ZH*SU(N)
      ZLR(N)=(ZLR(N)+ZJR(N))/4.0
      ZLU(N)=(ZLU(N)+ZJU(N))/4.0
      ERRRE(N)=ABS((ZJR(N)-ZJOR(N))/ZJR(N))
      ERRU(N)=ABS((ZJU(N)-ZJOU(N))/ZJU(N))
  132 CONTINUE
      DO 133 N=1,NF
      IF(ERRRE(N).GT.1.0E-4) GO TO 135
      IF(ERRU(N).GT.1.0E-4) GO TO 135
  133 CONTINUE
      WRITE (6,20) L
   20 FORMAT (/3H L=,I2)
      GO TO 137
  135 NN=2*NN
      ZH=ZH/2.0
  136 CONTINUE
      WRITE(6,33) N,ERRRE(N),ERRU(N)
   33 FORMAT(1H ,2HN=,I5,5X,9HERRRE(N)=,E15.8,5X,8HERRU(N)=,E15.8)
  137 DO 138 N=1,NF
      ZINTGR(N)=ZJR(N)/3.0
  138 ZINTGU(N)=ZJU(N)/3.0
      RETURN
      END
      SUBROUTINE FNCTN (FFQR,FFQU,H,AINC,NF,X)
      COMPLEX RUA,RUC,H1,H2,VBX,VBA,D90,H11,H22,HT
      COMPLEX HA,HA1,GOC
      DIMENSION FFQR(20),FFQU(20)
      PI=3.1415927
      TPI=2.0*PI
      FN=1.5
      PH180=180.000
      PH180R=PH180*PI/180.000
      PH90=90.0
      PH270=270.0
      D11=X+H
      D12=X*H/D11
```

```
      D13=SQRT(D11)
      D21=SQRT(H*H+X*X)
      D22=H+D21
      D23=D21*H/D22
      D24=SQRT(D22)
      PHA=ATAN2(X,H)*180.0/PI
      PHP=PH180+PHA
      CALL VB (RA,UA,D12,PH90,FN)
      CALL VB(RB,UB,D12,PH270,FN)
      CALL VB (RC,UC,D23,PHA,FN)
      CALL VB (RD,UD,D23,PHP,FN)
      RDUDM=SQRT(RD**2+UD**2)
      IF(X.EQ.0.0.AND.RDUDM.LT.0.5) RD=RD+COS(PI*H)
      IF(X.EQ.0.0.AND.RDUDM.LT.0.5) UD=UD-SIN(PI*H)
      IF(PHP.GT.182.0) GO TO 22
      WRITE(6,32) PHP,RD,UD
32    FORMAT(1H ,4HPHP=,F10.6,5X,2E15.8)
22    RUA=CMPLX(RA+RB,UA+UB)
      RUC=CMPLX(RC+RD,UC+UD)
      H1=CEXP(CMPLX(0.0,TPI*(D12-D11)))/D13*RUA
      H2=CEXP(CMPLX(0.0,TPI*(D23-D22)))/D24*RUC
      R2=SQRT(X*X+H*H)
      PH2=90.0+ATAN2(X,H)*180.0/PI
      CALL VB (RVB,UVB,R2,PH2,FN)
      CALL VB (RVB1,UVB1,X,PH180,FN)
      GOC=CEXP(CMPLX(0.0,-(TPI*X)))
      VBA=CMPLX(RVB1,UVB1)
      VBAM=SQRT(RVB1**2+UVB1**2)
      IF(VBAM.LT.0.5) VBA=VBA+GOC
      WRITE(6,19) X,VBA
19    FORMAT(1H ,2HX=,F10.6,5X,4HVBA=,2E15.8)
      VBX=VBA+CMPLX(RVB,UVB)
      D90=((1.0/FN*SIN(PI/FN))/(COS(PI/FN)-COS(PI/(2.0*FN))))*(CEXP(CMPL
     2X(0.0,-PI/4.0))/TPI)
      H11=D90*H1
      H22=D90*H2
      HT=VBX+H11+H22
      HTM=SQRT(REAL(HT)**2+AIMAG(HT)**2)
      HTP=180.0*ATAN2(AIMAG(HT),REAL(HT))/PI
      WRITE(6,20) X,HTM,HTP
20    FORMAT(1H ,2HX=,F10.6,5X,4HHTM=,E15.8,5X,4HHTP=,E15.8)
      DO 103 N=1,NF
      THETA=(FLOAT(N)-1.0)*AINC*PI/180.0
      IF(N.LT.4) THETA=THETA/2.0
      IF(N.EQ.5) THETA=FLOAT(N)*AINC*PI/180.0
      IF(N.EQ.6) THETA=FLOAT(N+1)*AINC*PI/180.0
      IF(N.EQ.7) THETA=2.0*PI/180.0
      HA1=CMPLX(0.0,TPI*COS(THETA))
      HA2=2.0*COS(TPI*SIN(THETA)*X)
      HA=HA1*HA2*HT
      FFQR(N)=REAL(HA)
      FFQU(N)=AIMAG(HA)
103   CONTINUE
104   RETURN
      END
```

APPENDIX B

The generalized Pauli series used in this analysis for diffraction of plane waves by a wedge was formulated by Hutchins and Kouyoumjian.[6] This appendix contains a brief summary of their results. Also included here is the wedge diffraction function subprogram which is used in the surface integration program presented in Appendix A.

The wedge geometry pertinent to the present discussion is shown in Fig. 12. The field diffracted from the wedge due to an incident plane wave is given by

$$U_d(\rho, \theta_i, \theta_d; n) = V_B(\rho, \theta_d - \theta_i, n) \pm V_B(\rho, \theta_d + \theta_i, n) \tag{31}$$

where the plus sign is for electric field polarization perpendicular to the edge of the wedge and the minus sign is for magnetic field polarization perpendicular to the edge of the wedge. The diffraction function V_B is given by

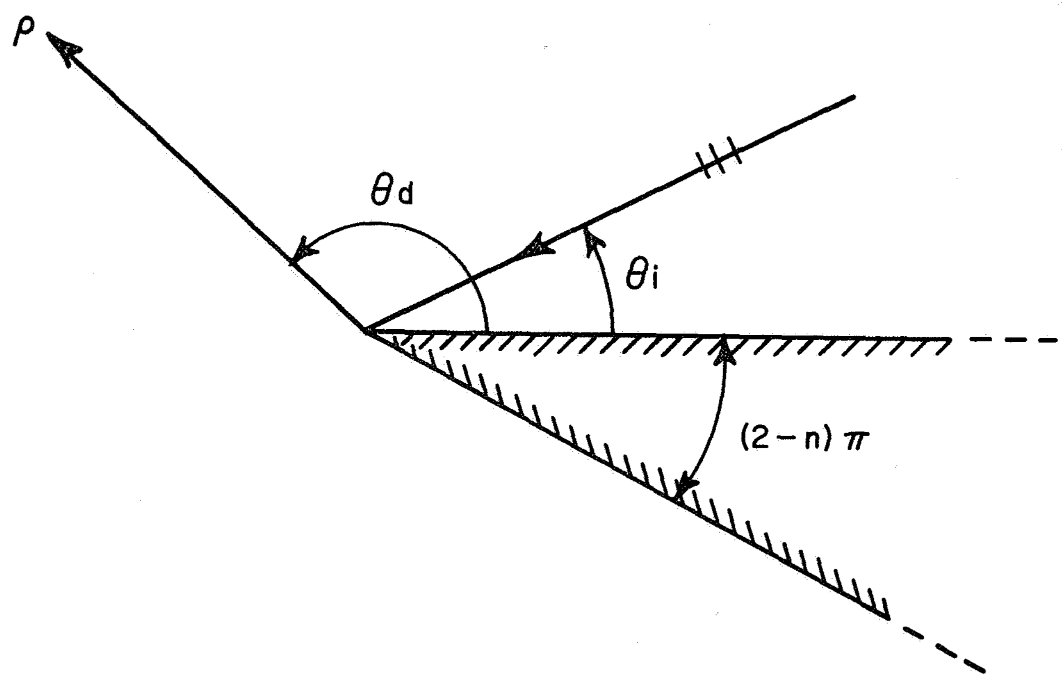

Fig. 12. Geometry of wedge diffraction.

(32) $$V_B(\rho, \beta; n) = I_{-\pi}(\rho, \beta; n) + I_{+\pi}(\rho, \beta; n)$$

where

(33) $$I_{\pm\pi}(\rho, \beta; n) \sim \frac{e^{-j\left(k\rho + \frac{\pi}{4}\right)}}{jn\sqrt{2\pi}} \sqrt{a} \cot\left(\frac{\pi \pm \beta}{2n}\right) e^{jk\rho a} \int_{(k\rho a)^{\frac{1}{2}}}^{\infty} e^{-j\tau^2} \, d\tau$$

with

$$a = 1 + \cos(\beta - 2n\pi N)$$

$$\beta = \theta_d \pm \theta_i \quad .$$

The number N is a positive or negative integer or zero which most nearly satisfies the equations

$$2n\pi N - \beta = -\pi \quad \text{for } I_{-\pi}$$

$$2n\pi N - \beta = +\pi \quad \text{for } I_{+\pi} \quad .$$

The above formulation maintains good accuracy for radial arguments as low as 0.2 wavelengths. For smaller arguments, the exact formulation based on an eigenfunction expansion may be used. This expansion, which converges rapidly for small arguments, is given by

(34) $$V_B(\rho, \phi; n) = \frac{1}{n} \sum_{m=0}^{\infty} \epsilon_m (j)^{\frac{m}{n}} J_{\frac{m}{n}}(k\rho) \cos \frac{m}{n} \phi$$

$$- \begin{cases} e^{jk\rho \cos\phi} & \phi < \pi \\ 0 & \phi > \pi \end{cases}$$

where

$$\epsilon_m = \begin{cases} 1 & m = 0 \\ 2 & m \neq 0 \end{cases} \quad .$$

The following Fortran IV subprogram was developed for evaluating the above V_B function. It is designed to switch automatically to the eigenfunction representation (using a finite sum approximation) for radial arguments less than 0.2 wavelengths. The Fresnel integral is evaluated in the subprogram by using the algorithm found by Boersma.[7]

```
      SUBROUTINE VB (RVB,UVB,R,ANG,FN)
      COMPLEX TERM,SUM
      COMPLEX DEM,TOP,COM,EXP,UPPI,UNPI
      DOUBLE PRECISION RAG,DP,TSIN
      PI=3.1415927
      TPI=2.0*PI
      ANG=ANG*PI/180.000
      IF (R.GT.0.2) GO TO 90
      IF(R.LT.0.001) NM=8
      IF(R.GE.0.001.AND.R.LT.0.01) NM=12
      IF(R.GE.0.01.AND.R.LT.0.1) NM=15
      IF(R.GE.0.1) NM=20
      ARG=TPI*R
      DEG=0.0
      IF(ARG.EQ.0.0) ANS=1.0
      IF(ANS.EQ.1.0) GO TO 14
      CALL BESSL (ANS,ARG,DEG)
   14 CONTINUE
      SUM=ANS/FN
      M=0
      DO 50 N=1,NM
      M=M+1
      CM=FLOAT(M)
      DEG=CM/FN
      IF(ARG.EQ.0.0) ANS=0.0
      IF(ANS.EQ.0.0) GO TO 17
      CALL BESSL (ANS,ARG,DEG)
   17 CONTINUE
      COM=2.0*ANS*CEXP(CMPLX(0.0,DEG*PI/2.0))
      TERM=COM*COS(DEG*ANG)/FN
      SUM=SUM+TERM
   50 CONTINUE
      IF(ANG.GT.-PI.AND.ANG.LT.PI) SUM=SUM-CEXP(CMPLX(0.0,TPI*R*COS(ANG)
     2))
      RVB=REAL(SUM)
      UVB=AIMAG(SUM)
      ANG=ANG*180.0/PI
      RETURN
   90 DEM=CMPLX(0.0,FN*SQRT(TPI))
      TOP=CEXP(CMPLX(0.0,-(TPI*R+PI/4.0)))
      COM=TOP/DEM
      N=IFIX((PI+ANG)/(2.0*FN*PI)+0.5)
      DN=FLOAT (N)
      A=1.0+COS(ANG-2.0*FN*PI*DN)
      BOTL=SQRT (TPI*R*A)
      EXP=CEXP(CMPLX(0.0,TPI*R*A))
      CALL FRNELS (C,S,BOTL)
      C=SQRT(PI/2.0)*(0.5-C)
      S= SQRT(PI/2.0)*(S-0.5)
      RAG=(PI+ANG)/(2.0*FN)
      TSIN=DSIN(RAG)
      TS=ABS(SNGL(TSIN))
      X=10.0
      Y=1.0/X**5
      IF(TS.GT.Y) GO TO 442
      COMP=-SQRT(2.0)*FN*SIN(ANG/2.0-FN*PI*DN)
      IF(COS(ANG/2.0-FN*PI*DN).LT.0.0) COMP=-COMP
      GO TO 443
  442 DP=SQRT(A)*DCOS(RAG)/TSIN
      COMP=SNGL(DP)
  443 UPPI=COM*EXP*COMP*CMPLX(C,S)
      N=IFIX((-PI+ANG)/(2.0*FN*PI)+0.5)
      DN=FLOAT(N)
      A=1.0+COS(ANG-2.0*FN*PI*DN)
```

```
      BOTL=SQRT(TPI*R*A)
      EXP=CEXP(CMPLX(0.0,TPI*R*A))
      CALL FRNELS (C,S,BOTL)
      C=SQRT(PI/2.0)*(0.5-C)
      S= SQRT(PI/2.0)*(S-0.5)
      RAG=(PI-ANG)/(2.0*FN)
      TSIN=DSIN(RAG)
      TS=ABS(SNGL(TSIN))
      IF(TS.GT.Y) GO TO 542
      COMP= SQRT(2.0)*FN*SIN(ANG/2.0-FN*PI*DN)
      IF(COS(ANG/2.0-FN*PI*DN).LE.0.0) COMP=-COMP
      GO TO 123
542   DP=SQRT(A)*DCOS(RAG)/TSIN
      COMP=SNGL(DP)
123   UNPI=COM*EXP*COMP*CMPLX(C,S)
      ANG=ANG*180.0/PI
      RVB=REAL (UPPI+UNPI)
      UVB=AIMAG(UPPI+UNPI)
      RETURN
      END
      SUBROUTINE FRNELS (C,S,XS)
      DIMENSION A(12),B(12),CC(12),D(12)
      A(1)=1.595769140
      A(2)=-0.000001702
      A(3)=-6.808568854
      A(4)=-0.000576361
      A(5)=6.920691902
      A(6)=-0.016898657
      A(7)=-3.050485660
      A(8)=-0.075752419
      A(9)=0.850663781
      A(10)=-0.025639041
      A(11)=-0.150230960
      A(12)=0.034404779
      B(1)=-0.000000033
      B(2)=4.255387524
      B(3)=-0.000092810
      B(4)=-7.780020400
      B(5)=-0.009520895
      B(6)=5.075161298
      B(7)=-0.138341947
      B(8)=-1.363729124
      B(9)=-0.403349276
      B(10)=0.702222016
      B(11)=-0.216195929
      B(12)=0.019547031
      CC(1)=0.0
      CC(2)=-0.024933975
      CC(3)=0.000003936
      CC(4)=0.005770956
      CC(5)=0.000689892
      CC(6)=-0.009497136
      CC(7)=0.011948809
      CC(8)=-0.006748873
      CC(9)=0.000246420
      CC(10)=0.002102967
      CC(11)=-0.001217930
      CC(12)=0.000233939
      D(1)=0.199471140
      D(2)=0.000000023
      D(3)=-0.009351341
      D(4)=0.000023006
      D(5)=0.004851466
      D(6)=0.001903218
```

```
      D(7)=-0.017122914
      D(8)=0.029064067
      D(9)=-0.027928955
      D(10)=0.016497308
      D(11)=-0.005598515
      D(12)=0.000838386
      IF(XS.LE.0.0) GO TO 414
      X=XS
      X=X*X
      FR=0.0
      FI=0.0
      K=13
      IF(X-4.0) 10,40,40
10    Y=X/4.0
20    K=K-1
      FR=(FR+A(K))*Y
      FI=(FI+B(K))*Y
      IF(K-2) 30,30,20
30    FR=FR+A(1)
      FI=FI+B(1)
      C=(FR*COS(X)+FI*SIN(X))*SQRT(Y)
      S=(FR*SIN(X)-FI*COS(X))*SQRT(Y)
      RETURN
40    Y=4.0/X
50    K=K-1
      FR=(FR+CC(K))*Y
      FI=(FI+D(K))*Y
      IF(K-2) 60,60,50
60    FR=FR+CC(1)
      FI=FI+D(1)
      C=0.5+(FR*COS(X)+FI*SIN(X))*SQRT(Y)
      S=0.5+(FR*SIN(X)-FI*COS(X))*SQRT(Y)
      RETURN
414   C=-0.0
      S=-0.0
      RETURN
      END
      SUBROUTINE BESSL (ANS,ARG,DEG)
      FAC=(0.5*ARG)**DEG
      XK=1.0
      ANS=0.0
      TOP=-0.25*(ARG**2)
      DO 43 K=0,10
      CK=FLOAT(K)
      YOP=TOP**K
      XK=XK*CK
      IF(XK.LT.1.0) XK=1.0
      BB=DEG+CK+1.0
      CALL GAMMA (BB,AC,IER)
      TERM=(YOP/XK)/AC*FAC
      ATERM=ABS(TERM)
      IF(ATERM.LT.1.0E-30) GO TO 44
      ANS=ANS+TERM
43    CONTINUE
44    RETURN
      END
      SUBROUTINE GAMMA(XX,GX,IER)
      X=XX
      ERR=1.0E-06
      IER=0
      GX=1.0
      IF(X-2.0) 50,50,15
   10 IF(X-2.0) 110,110,15
   15 X=X-1.0
```

```
      GX=GX*X                                                           GAMMA040
      GO TO 10                                                          GAMMA041
   50 IF(X-1.0) 60,120,110                                              GAMMA042
   60 IF(X-ERR) 62,62,80                                                GAMMA046
   62 Y=FLOAT(INT(X))-X                                                 GAMMA047
      IF(ABS(Y)-ERR) 130,130,64                                         GAMMA048
   64 IF(1.0-Y-ERR) 130,130,70                                          GAMMA049
   70 IF(X-1.0) 80,80,110                                               GAMMA053
   80 GX=GX*X                                                           GAMMA054
      X=X+1.0                                                           GAMMA055
      GO TO 70                                                          GAMMA056
  110 Y=X-1.0                                                           GAMMA057
      GY=1.0+Y*(-0.5771017+Y*(+0.9858540+Y*(-0.8764218+Y*(+0.8328212+   GAMMA058
     1Y*(-0.5684729+Y*(+0.2548205+Y*(-0.05149930)))))))                 GAMMA059
      GX=GX*GY                                                          GAMMA060
  120 RETURN                                                            GAMMA061
  130 IER=1                                                             GAMMA062
      RETURN                                                            GAMMA063
      END                                                               GAMMA064
```

REFERENCES

1. Rudduck, R.C., "Application of Wedge Diffraction to Antenna Theory," Report 1691-13, 30 June 1965, Antenna Laboratory, The Ohio State University Research Foundation; prepared under Grant NsG-448, National Aeronautics and Space Administration, Office of Grants and Research Contracts, Washington, D.C.

2. Ryan, C.E., Jr., and Rudduck, R.C., "Calculation of the Radiation Pattern of a General Parallel-Plate Waveguide Aperture for the TEM and TE_{01} Waveguide Modes," Report 1693-4, 10 September 1964, Antenna Laboratory, The Ohio State University Research Foundation; prepared under Contract N62269-2184, U.S. Naval Air Development Center, Johnsville, Pennsylvania.

3. Yu, J.S. and Rudduck, R.C., "Higher-Order Diffraction Concept Applied to Parallel-Plate Waveguide Patterns," Report 1691-16, 15 October 1965, Antenna Laboratory, The Ohio State University Research Foundation; prepared under Grant NsG-448, National Aeronautics and Space Administration, Office of Grants and Research Contracts, Washington, D.C.

4. Wu, D.C.F., "The TEM Radiation Pattern of a Thin-Walled Parallel-Plate Waveguide Analyzed by a Surface Integration Technique," Report 1691-23, 20 September 1967, ElectroScience Laboratory, The Ohio State University Research Foundation; prepared under Grant NsG-448, National Aeronautics and Space Administration, Office of Grants and Research Contracts, Washington, D.C.

5. Nussenzveig, H. M., "Solution of a Diffraction Problem. I - The Wide Double Wedge. II - The Narrow Double Wedge," Phil. Trans. Roy. Soc., London, Ser. A, Vol. 252, (October 15, 1959) pp. 1-51.

6. Hutchins, D.L., and Kouyoumjian, R.G., "A New Asymptotic Solution to the Diffraction by a Wedge," URSI 1967 Spring Meeting, Ottawa, Canada, pp. 154-155.

7. Boersma, J., "Computation of Fresnel Integrals," Math. Comp., Vol. 14, (1960), p. 380.